Bioconjugate Chemistry

Article

pubs.acs.org/bc

Dual Mode Fluorescent ^{18}F-PET Tracers: Efficient Modular Synthesis of Rhodamine-[cRGD]$_2$-[^{18}F]-Organotrifluoroborate, Rapid, and High Yielding One-Step ^{18}F-Labeling at High Specific Activity, and Correlated *in Vivo* PET Imaging and *ex Vivo* Fluorescence

Zhibo Liu,[†] Mark Alex Radtke,[†] May Q. Wong,[‡] Kuo-Shyan Lin,[§] Donald T. Yapp,[‡] and David M. Perrin*[,†]

[†]Chemistry Department University of British Columbia 2036 Main Mall, Vancouver, British Columbia V6T-1Z1, Canada

[‡]Experimental Therapeutics and [§]Molecular Oncology, B.C. Cancer Agency 675 West 10th Avenue Vancouver, British Columbia V5Z-1L3, Canada

Supporting Information

ABSTRACT: The design of dual mode fluorescent-PET peptidic tracers that can be labeled with [^{18}F]fluoride at high specific activity and high yield has been challenged by the short half-life of ^{18}F and its aqueous indolence toward nucleophilic displacement, that often necessitates multistep reactions that start with punctiliously dry conditions. Here we present a modular approach to constructing a fluorescent dimeric peptide with a pendant radioprosthesis that is labeled in water with [^{18}F]fluoride ion in a single, user-friendly step. The modular approach starts with grafting a new zwitterionic organotrifluoroborate radioprosthesis onto a pentaerythritol core with three pendent alkynes that enable successive grafting of a bright fluorophore (rhodamine) followed by two peptides (cylcoRGD). The construct is labeled with [^{18}F]fluoride via isotope exchange within 20 min in a single step at high specific activity (>3 Ci/μmol) and in good yield to provide 275 mCi and high radiochemical purity. Neither drying of the [^{18}F]fluoride ion solution nor HPLC purification of the labeled tracer is required. Facile chemical synthesis of this dual mode tracer along with a user-friendly one-step radiolabeling method affords very high specific activity. In vivo PET images of the dual mode tracer are acquired at both high and low specific activities. At very high specific activity, i.e., 3.5 Ci/μmol, tumor uptake is relatively high (5.5%ID/g), yet the associated mass is below the limits of fluorescent detection. At low specific activity, i.e., 0.01 Ci/μmol, tumor uptake in the PET image is reduced by approximately 50% (2.9%ID/g), but the greater associated mass enables fluorescence detection in the tumor. These data highlight a facile production of a dual mode fluorescent-PET tracer which is validated with *in vivo* and *ex vivo* images. These data also define critical limitations for the use of dual mode tracers in small animals.

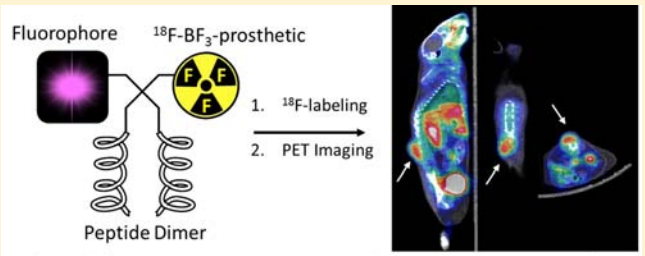

Dual Mode Fluorescent PET Tracers: ◘ Modular Construction, ◘ Synthetic Efficiency, ◘ Peptide Dimerization for High Affinity, ◘ One-step ^{18}F-Labeling, ◘ High Specific Activity ◘ Functional PET Imaging, ◘ Ex-vivo Fluorescence

INTRODUCTION

Molecular imaging is at the forefront of translational medicine. Of the various imaging modalities, both PET (positron emission tomography) and fluorescence imaging are increasingly used in preclinical and clinical applications. Given the interest in both modalities, a single molecular entity that combines both a fluorophore and a radioprosthesis would facilitate several bench-to-clinic applications.[1−6] The key advantage of a dual-mode tracer is that the *same* molecule has the potential to function as a fluorescent probe for *ex vivo* histopathology and/or fluorescent-guided surgeries,[7,8] and as a PET tracer for pre- and postoperative staging in the same patient. Whereas there have been several reports of fluorescent peptides that have been labeled by radiometalation,[9−11] examples of ^{18}F-labeled fluorescent tracers are scant, perhaps owing to the challenges of ^{18}F-labeling in high yield and high specific activity.[12−14]

Toward these ends, direct ^{18}F-labeling of two (Bodipy) fluorophores was elegantly achieved either by displacement of DMAP from boron in water[15,16] or of OTf from boron[16] in very dry solvent as noted in one report, or by Lewis acid promoted ^{19}F−^{18}F-isotope exchange (IEX) as noted in another.[17,18] In each case, the [^{18}F]-Bodipy, as an NHS-ester, was conjugated to a peptide or antibody in a second step.[16] In the case of the former, tumor uptake was imaged by PET and correlated with *ex vivo* fluorescence. In contrast to these examples that require two radiosynthetic steps, an antecedent

Received: July 25, 2014
Revised: September 4, 2014
Published: September 29, 2014

   dx.doi.org/10.1021/bc5003357 | *Bioconjugate Chem.* 2014, 25, 1951−1962

Scheme 1. Synthetic Route for the Modular and Rapid Construction of a Dual Mode Fluorescent-PET Tracer with a Dimeric Peptide

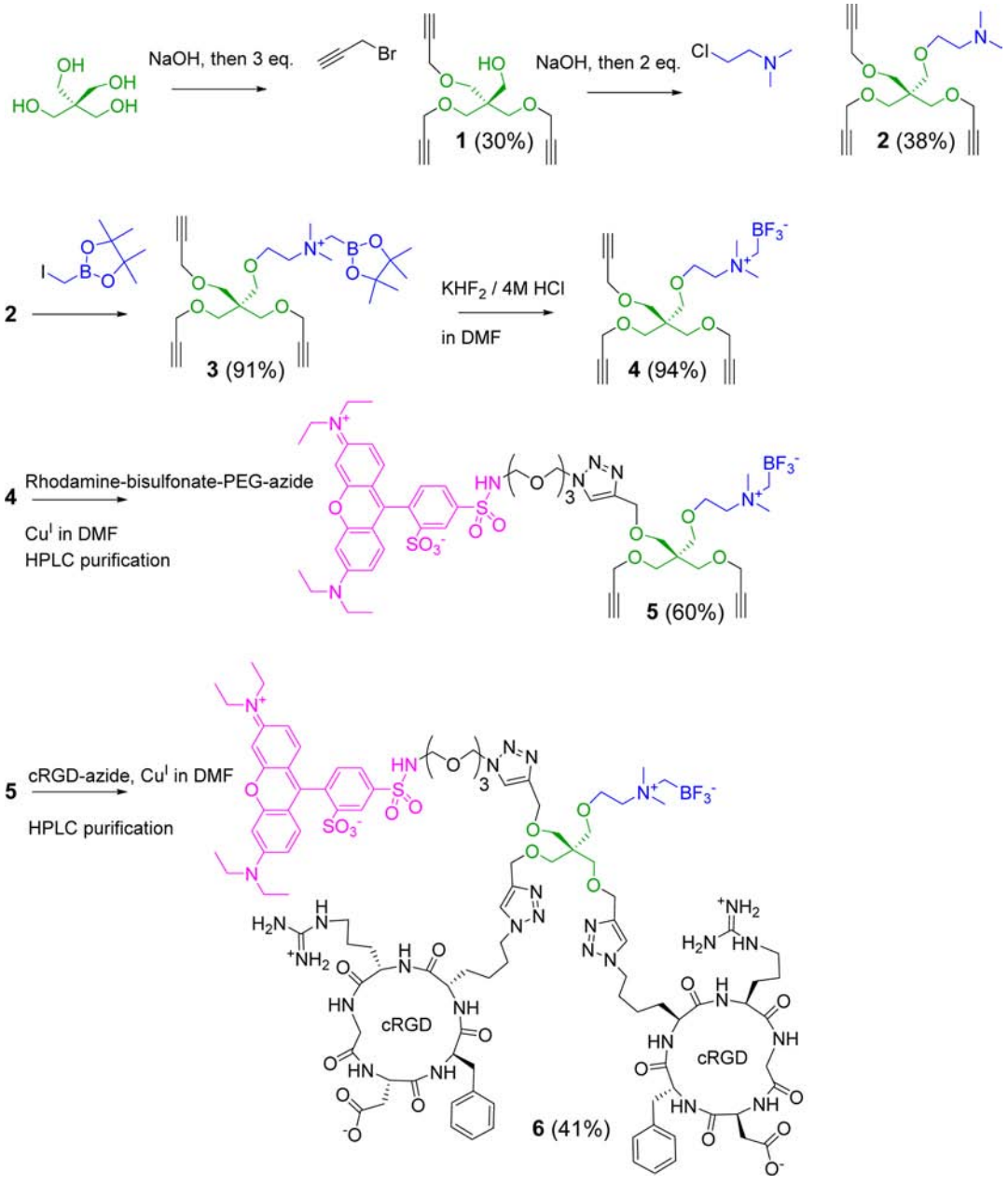

publication described ^{18}F-labeling of a macromolecule Lymphoseek to which was conjugated an arylboronic ester that had been first conjugated to a Cy7 fluorophore. Labeling proceeded in a single aqueous step and gave impressive images of the sentinel lymph node in both fluorescent and PET modes.[19] Notably in all three cases, the specific radioactivity values of these ^{18}F-labeled fluorescent tracers[9,10] were useful ($\leq$0.05 Ci/μmol) yet low enough to provide enough mass for correlated *ex vivo* fluorescence and PET imaging.

Nevertheless, high specific activity (i.e., >2 Ci/μmol), with low associated mass, may be needed to provide high contrast PET images, and more importantly will be required to meet FDA regulatory guidelines concerning microdose requirements.[12,20,21] The advantages of high specific activity have been reviewed at length.[22−24] Yet to date, the production of a dual mode fluorescent ^{18}F-radiotracer at very high specific activity has, to the best of our knowledge, never been reported.

Herein we report the synthesis of a fluorescent peptide tracer that is ^{18}F-labeled in a single aqueous step in high yield and at high specific activity and is obtained within 30 min *without* HPLC purification. The convergent synthetic strategy is flexible as it lets radiochemists and clinicians choose from any number of fluorophores without restriction to a bodipy chromophore for ^{18}F-labeling. Moreover, the one-step radiosynthesis at high specific activity in turn enables the evaluation of tumor-specific *in vivo* PET images and *ex vivo* tumor visualization by fluorescence to validate dual mode imaging. The synthetic and radiosynthetic aspects of this approach along with the resulting *in vivo* PET data and *ex vivo* fluorescent data are reported.

dx.doi.org/10.1021/bc5003357 | *Bioconjugate Chem.* 2014, 25, 1951−1962

RESULTS

In terms of a bioconjugation strategy, we sought a facile and modular construction for generating a tracer that comprises a peptide-dimer for increased affinity,[25,26] a bright fluorophore of choice, and an ^{18}F-radioprosthesis. In terms of a radioprosthesis, we sought one that would afford an efficient late-stage labeling that would proceed in a single, aqueous step via a user-friendly method that obviates both drying of the [^{18}F]-fluoride ion prior to labeling and HPLC purification following. Previously we showed that aryltrifluoroborates are labeled in a single aqueous step in high yield and at high specific activity.[27−29] With production-levels of [^{18}F]fluoride ion (>500 mCi), isotope exchange (IEX) can be used to prepare various [^{18}F]ArBF$_3^-$ conjugates.[28−30] Here we feature a new zwitterionic radioprosthesis, ammoniomethyltrifluoroborate (AMBF$_3$), which is considerably more stable *in vitro*. Because IEX labeling does not change the composition of the radiotracer, HPLC purification is replaced by a simple C18-SepPak elution to give several hundred millicuries of radiochemically pure ^{18}F-labeled tracer.

Whereas we could have chosen any number of peptides that have been conjugated to various prosthetic groups and probes, here we chose cyclic RGD (cRGD) for two important reasons: (1) there is an abiding interest in labeling and imaging dimeric cRGD in humans as evidenced by recent publications that report clinical applications;[31,32] (2) cRGD is not an experimental tracer and hence we avoid variables such as *in vivo* stability and target specificity in order to focus on radiosynthetic parameters, specific activity characteristics, and *in/ex vivo* data in comparison with antecedent dimeric cRGD tracers.[33]

Of the many fluorophores that can be conjugated to peptides, we chose rhodamine based on several attractive properties: (1) *in vivo* stability; (2) compatibility with most microscope fluorescent cube sets, scanners, fluorimeters, and spectrophotometers; (3) a longer emission wavelength ($\lambda_{em.}$ = 584 nm) compared to aforementioned [^{18}F]Bodipy fluorophores (($\lambda_{em.}$ = 503 or 547 nm);[17,18,30] and (4) brightness due to a high quantum yield (ϕ = 0.56)[34] that is ∼5-fold higher than the IR dye: IR-Dye800-CW.[35] Additionally, a very high molar extinction coefficient (ε = 100 000 M^{-1} cm^{-1}, λ_{max} = 568 nm) enables accurate measurement of tracer concentration by UV−vis spectroscopy in order to determine specific activity.[28,29] Finally, we opted for "click" conjugation for synthetic construction due to its broad utility in bioconjugation[36−38] and recent applications to radiotracers.[39,40]

Based on these considerations, synthesis commenced with 3-fold propargylation of pentaerythritol followed by treatment with *N,N*-dimethyl-*N*-(chloroethyl)amine. The amine was quaternized with iodomethylboronyl pinacolate to give **3**, *N,N*-dimethyl-ammonio-*N*-methyl-boronyl pinacolate, which was converted to the trifluoroborate in the presence of KHF$_2$ to give **4**. Cpd **4** could be grafted to a fluorophore-azide of choice to give **5**. To do this cleanly, **4**, in excess (2−3 equiv), was treated with 1 equiv commercially available rhodamine-PEG-azide in the presence of cuprous ion to give **5** with two pendant alkynes for subsequent peptide grafting while unreacted **4** was recovered and recycled. Cpd **5** represents a novel "radiosynthon" which *a priori* should be amenable to grafting peptides as needed. For "click" conjugation, cRGD-N$_3$ in slight excess (2.5 equiv) as previously prepared[41] was combined with 1 equiv of **5** in the presence of cuprous ion to provide the desired radiotracer precursor **6** (Scheme 1) that can be labeled by IEX. The conversion of **3** to **6** was achieved in reasonable yields to provide ∼10 mg that can be used for ∼70 labeling reactions. Following HPLC purification, purity was confirmed by MALDI-TOF (see Supporting Information). A solution of **6** in EtOH was aliquoted in quantities of 30, 50, or 75 nmol, dried, and stored at −20 °C for on-demand kit labeling.

As the purpose of this work was to address the production of a dual mode tracer and because target binding is typically not in doubt with RGD dimers, we did not measure an apparent K_d/IC$_{50}$. Moreover, tumor uptake values are but loosely correlated with K_d values as some ligands with low apparent affinity can still provide high contrast images with good tumor uptake (>5% ID/g). More importantly, target-specific binding was qualitatively confirmed by fluorescence microscopy on cells that did or did not express the $\alpha_v\beta_3$ integrin receptor (Figure 1A,B).

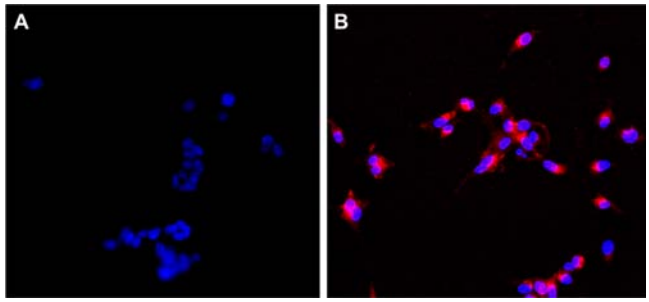

Figure 1. Fluorescent microscopy of $\alpha_v\beta_3$ integrin binding: (A) negative control with HT29 cells (**6** at 960 nM); (B) positive control with U87 M cells (**6** at 480 nM). The red halo surrounding U87 M cell nuclei is due to rhodamine as expected. DAPI (blue) stains nuclei in both panels. Cells were washed briefly before plating.

For radiolabeling, NCA (no carrier added) [^{18}F]fluoride ion was obtained by (i) bombardment of H$_2^{18}$O with 18 MeV protons, (ii) concentration by anion exchange, and (iii) direct elution with 70−100 μL saline into a tube containing **6** in 50% buffered DMF/H$_2$O. The labeling reaction was heated (85 °C) for 20 min and then quenched with 5% NH$_4$OH in EtOH (1 mL). The crude reaction was then passed over a C18-SepPak (pretreated first with MeCN and then water), washed with 2 mL saline, and eluted into 0.5 mL of 1:1 ethanol−PBS in yields of 13−33% (Figure 2A) (n = 3, see Supporting Information for radiosynthetic data of each run). For imaging, [^{18}F]**6** was further diluted in PBS (5−10 mL).

On the day of imaging, IEX labeling was effected by reacting 75 nmol **6** (180 μg) with 809 mCi NCA [^{18}F]fluoride ion to provide 275 mCi of radiochemically pure [^{18}F]**6** in less than 25 min without HPLC purification (33% RCY not corrected for decay). From this labeling reaction, 5 mCi was removed, packaged, and transported for tail vein injections. Simultaneously, an aliquot (∼100 μL, 1.8 mCi) was injected onto an analytical RP-C18 HPLC column to obtain a quality control HPLC radiochromatogram to confirm radiochemical purity (Figure 2B). The correlated UV−vis trace (Figure 2C) was recorded at 568 nm. Notably, both traces demonstrate extremely high radiochemical and chemical purity. To assay stability, the tracer was incubated in mouse serum at 37 °C for 0, 60, and 120 min with no apparent degradation at 120 min, a period of time equal to the imaging time window (see Supporting Information).

dx.doi.org/10.1021/bc5003357 | *Bioconjugate Chem.* 2014, 25, 1951−1962

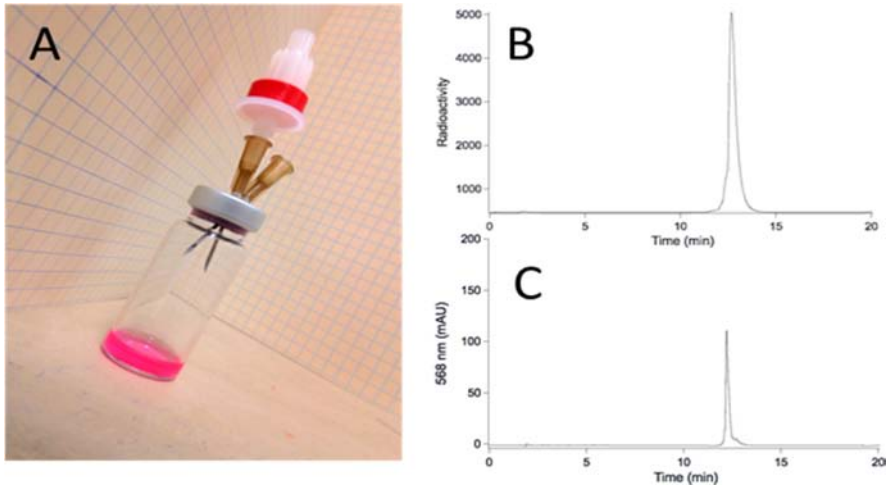

Figure 2. (A) [^{18}F]**6** following elution from Sep-Pak in 50% ethanol-PBS in vial (275 mCi); (B) QC radiotrace of 1.8 mCi of Sep-Pak eluted tracer; (C) UV-trace at 568 nm of the same sample.

Use of a standard curve (see Supporting Information) established that the 1.8 mCi that eluted comprised a quantity of 0.46 nmol **6**. Hence the specific activity was measured at 3.95 Ci/μmol at the time of elution. Within experimental error of 10%, this value is consistent with the calculated specific activity (275 mCi/75 nmol = 3.6 Ci/μmol).

Whereas PET tracers are typically imaged at high specific activity, dual mode tracers are typically imaged at very low specific activity.[9,10,18,19,42,43] Here, the production of [^{18}F]**6** at very high specific activity allowed us to deliver the same tracer at low specific activity simply by diluting it with precursor [^{19}F]**6**. This enabled us to address the effect of specific activity (high or low) in terms of imaging in both modes, with the expectation that at low specific activity, blocking of specific uptake would be observed. Within 10 min of isolation, 100 μCi of [^{18}F]**6** was injected into mice in which U87 M glioblastoma tumor xenografts had been grown to 70−100 mm^3 (70−100 mg). With only a 10 min delay between packaging and injection, the specific activity of [^{18}F]**6** following packaging fell to 3.5 Ci/μmol (corrected for ~10 min delay). For delivery at low specific activity, [^{18}F]**6** was simply diluted first with 10 nmol of [^{19}F]**6**, (100 μCi/10 nmol = 0.01 Ci/μmol). In each case (high SA or low SA), [^{18}F]**6** cleared predominantly to the bladder (>90% ID/g) via the kidneys with some uptake in liver and minimal uptake in bone (Figure 3 and Figure 5 *vide infra*).

As the $AMBF_3$ radioprosthesis is new, we were concerned with the slightly elevated uptake in bone (~1.7%) as shown in Figure 3: This slightly elevated value for bone uptake suggests either that the $AMBF_3$ radioprosthesis is not metabolically stable in blood or that there is specific uptake in bone. Notably, bone uptake is partially blocked at low specific activity, even to a greater extent than what is seen in the tumor. Such would indicate specific uptake due to integrin receptors that are known to be expressed in bone tissue.[44,45] If defluoridation had occurred, the apparent uptake of free fluoride in bone could not be blocked because bone is not saturable with fluoride. To further address this, time−activity curves (TACs) were also generated based on the PET image (Figure 4).

The TAC data show that bone uptake falls over time, an observation which is also consistent with metabolic stability. Finally, while some bone structure along with other organs are observed in the PET-alone image of the unblocked animal, systemic partial blocking is observed in the image that was

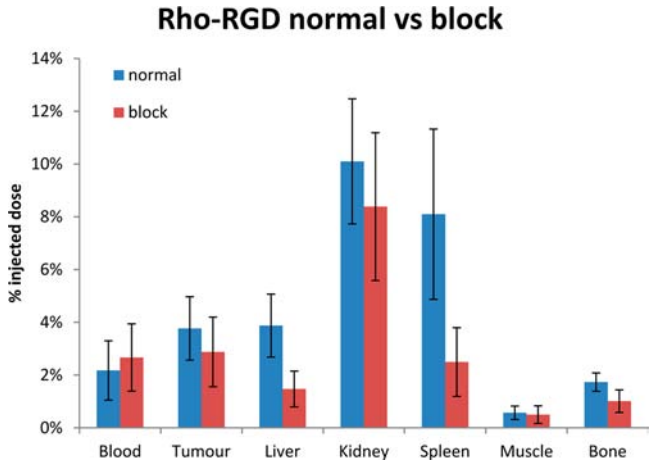

Figure 3. Biodistribution data of key organs following sacrifice of animals (n = 4).

acquired at low specific activity which further supports the argument that uptake in bone and other nontumor organs is specific for the $\alpha_v\beta_3$ target that is expressed at low levels throughout the mouse (Figure 5A,B). Taken together, post-mortem biodistribution data, TAC data, and the apparent systemic blocking in the PET images suggest that the $AMBF_3$ is stable *in vivo*. Hence we turned our attention to specific tumor uptake and the correlation thereof with *ex vivo* fluorescence imaging.

To begin, the mouse that received 100 μCi of [^{18}F]**6** at 3.5 Ci/μmol (30 pmol total **6**) showed uptake in tumor (Figure 5A,B, left mouse), scaled at 5.5% ID/g in 2D images (Figure 5B). This value is corroborated by post mortem tissue analysis, which gave an uptake value of 3.8 ± 1.2% ID/g (n = 3) in tumor. The mouse that received 100 μCi of [^{18}F]**6** at 0.01 Ci/μmol showed 2-fold lower uptake in tumor, which is scaled to 2.5% ID/g (Figure 5A,B, right mouse), and is corroborated by post mortem tissue analysis that gave a value of 2.9 ± 1.2% ID/g. Because of the way mice were laid in the scanner, it was essential to provide three different views (coronal, sagittal, and transverse) of each mouse to better illustrate the partial blocking that occurs systemically.

Despite an injected dose of 10 nmol [^{19}F]**6**, it is not surprising that blocking was incomplete. In fact, statistically

dx.doi.org/10.1021/bc5003357 | *Bioconjugate Chem.* 2014, 25, 1951−1962

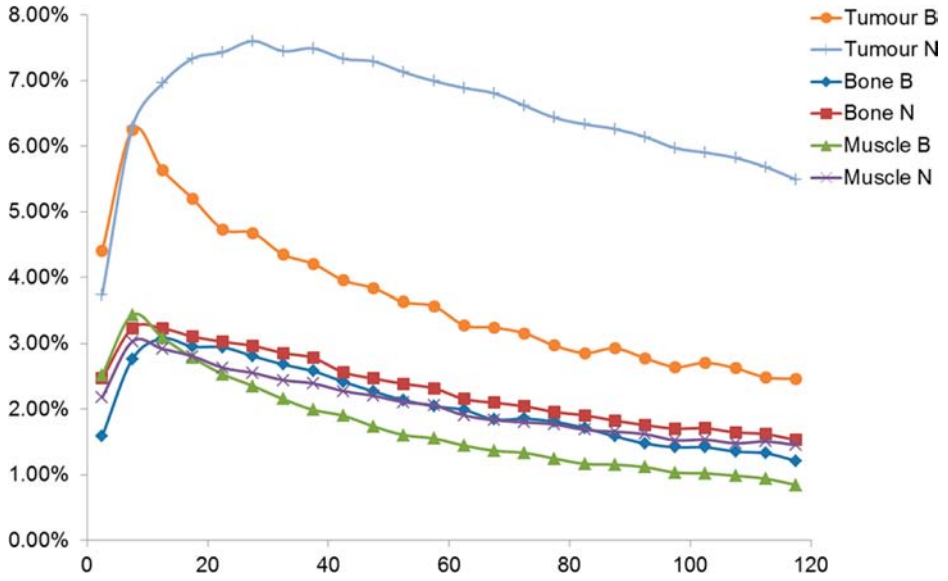

Figure 4. TAC (time−activity curve) data for the two mice that were imaged: *N* = blocked, B = blocked, *y*-axis is %ID/g and *x*-axis is time (min).

significant blocking of the $\alpha_v\beta_3$ receptor typically requires injection of 40−150 nmol of RGD.[46−48] Nevertheless, because partial blocking was achieved with [^{19}F]**6**, the interaction must be specific for **6**. Yet *a priori* we cannot know for sure if the apparent specificity is due to the dimeric cRGD peptides, the $AMBF_3$ radioprosthesis, or the rhodamine. It would especially exciting if the observed uptake were simply due to the radioprosthesis and not the cRGD! Although very unlikely, were that to be the case, the conclusions of this work in terms of the limits of fluorescent detection would remain unchanged. For reasons that will become evident in the Discussion section, we deliberately chose to perform a partial blocking experiment at a specific activity that was just low enough to afford partial blocking yet high enough to ensure still-detectable uptake in the tumor. Hence the very low specific activity value, i.e., 0.01 Ci/μmol, was chosen because it is consistent with other reports on dual mode fluorescent PET tracers and would ultimately allow us to correlate lower uptake values with fluorescence detection.

Following PET scanning, we explored fluorescent imaging *ex vivo* to visualize uptake of **6** at both high and low specific activity (Figure 6B,C, respectively). With 100 μCi (30 pmol) injected and uptake at 5.11% ID/g measured in the actual tumor sample that was removed, the particular tumor section, which weighed 39 mg, therefore contains ∼60 fmol of tracer (actually 56.9 fmol from arithmetic analysis). Although fluorescence can be used to detect single molecules, such studies require highly specialized optics that are ill-suited for whole tissue examination or fluorescence-guided surgery. Indeed, with a camera dedicated to tissue imaging, we were unable to detect <10 pmol of **6** in 100 μL pure water in which no quencher is present (data not shown). Hence, not surprisingly, no fluorescence was detected in a tumor slice containing 60 fmol (Figure 6B), compared to a control that received no tracer (Figure 6A).

For the mouse that received 100 μCi [^{18}F]**6** at ∼0.01 Ci/μmol (10 nmol), an uptake value of 3.8% ID/g in the specific tumor sample, which weighed 45 mg, corresponds to 17 pmol of **6**. This significantly larger amount results from injecting a much greater mass, which in turn reflects a 300-fold lower specific activity. Gratifyingly, fluorescence was observed in this case (Figure 6C). Similarly, fluorescence in liver, and to a lesser extent in kidney, is attenuated due to the presence of tissue-specific quenchers (e.g., porphyrins) that may absorb either the incident photon for excitation or that of fluorescence emission. The results from both PET and fluorescence imaging herein are summarized in Table 1.

The data from the low specific activity injection are consistent with the report of [^{18}F]Bodipy-cRGD labeled at 0.05 Ci/μmol that afforded fluorescent *ex vivo* images and similar uptake values by PET (no blocking experiment was performed in that particular study as the specificity of RGD for the integrin receptor is not in doubt).[18] The relatively high chemical amounts of fluorescent tracer needed to observe fluorescence is also consistent with reports on dual-mode near-IR-fluorophore-RGD tracers labeled with radiometals that are injected at specific radioactivities ≤0.05 Ci/μmol in order to show correlated uptake by PET and fluorescence.[9,10,42,43]

DISCUSSION

To the best of our knowledge, this work represents the first report of a functional dual-mode ^{18}F-fluorescent PET tracer that is labeled *and* PET imaged at high specific activity (>3 Ci/μmol). The ability to routinely achieve high specific activity is a consequence of using isotope exchange, along with an organotrifluoroborate radioprosthesis that affords rapid, one-step labeling. Hence, we were able to dilute the radiotracer with the unlabeled fluorescent isotopolog (precursor) to investigate PET imaging and fluorescent detection at very low specific activity as well.

With an injected dose of 100 μCi of [^{18}F]**6** at 3.5 Ci/μmol, the total injected mass (30 pmol) is *far below* levels used in fluorescent probe studies.[6,49−54] At least in our hands (with a Maestro-2 camera system), 10 pmol of **6** in pure water represents the limit of fluorescence detection in a medium in which there are no tissue-specific quenchers (e.g., porphyrins). Detection limits in pure water are generally a function of camera sensitivity and fluorophore brightness and are independent of emission wavelength. Hence while near-IR dyes and other fluorophores may improve tissue penetration, the fundamental limits of detection in water will not be improved with near IR fluorophores. Therefore, our inability to

dx.doi.org/10.1021/bc5003357 | *Bioconjugate Chem.* 2014, 25, 1951−1962

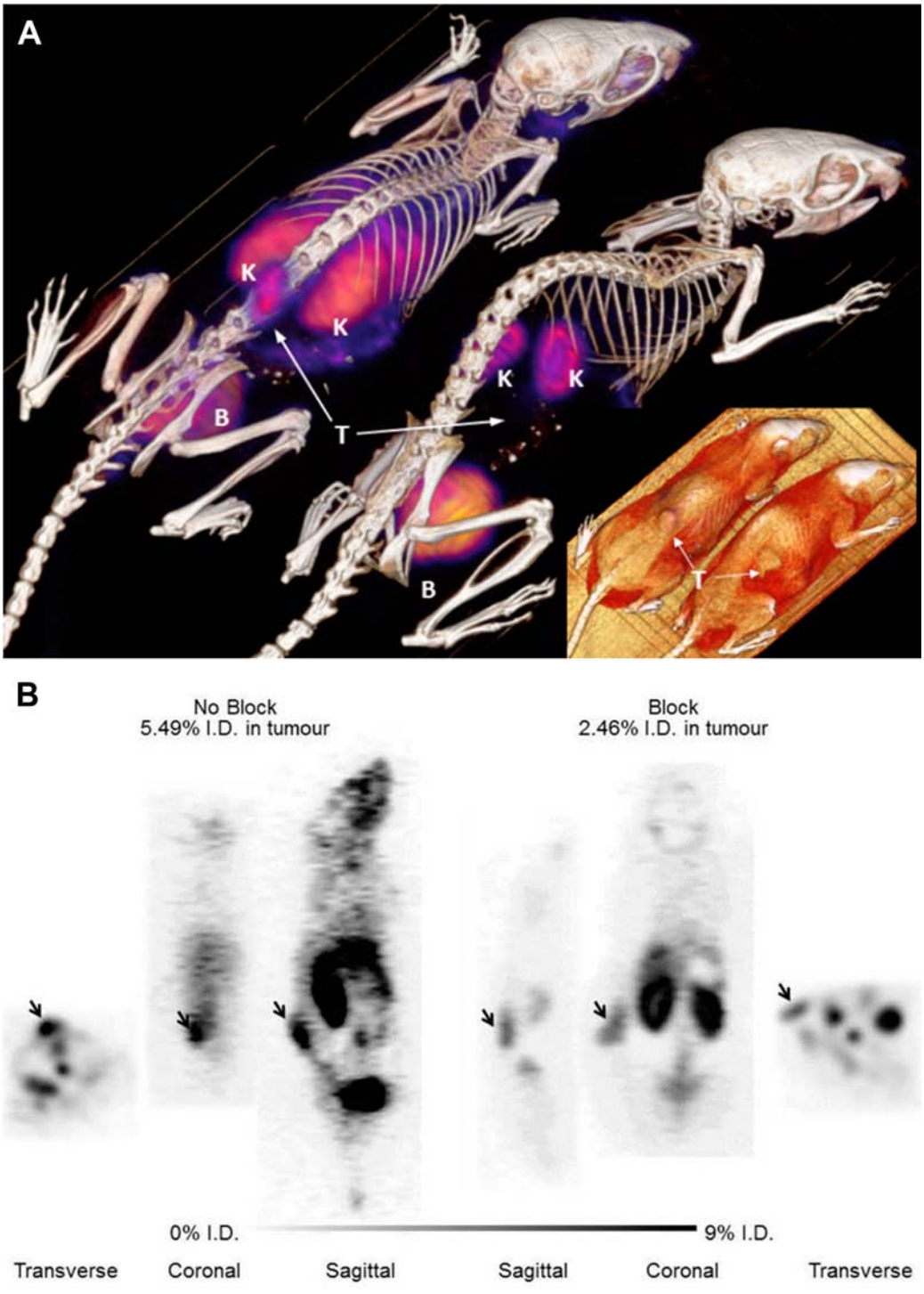

Figure 5. (A) 3D PET-CT images: T (tumor), K (kidney), B (bladder), left mouse imaged with [^{18}F]**6** at 3.5 Ci/μmol, right mouse imaged with [^{18}F]**6** at 0.01 Ci/μmol (3D rendering augments the extent of blocking); inset bottom right: CT-alone image showing tumors. (B) 2D PET-alone image with scale bar of the same mice with three slices and %ID/g values in tumor (left slices are unblocked, right slices "blocked" by the addition of 10 nmol [^{19}F]**6**).

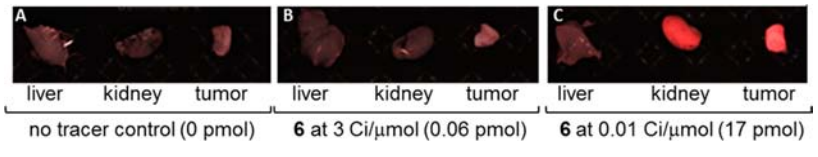

Figure 6. *Ex vivo* fluorescence in organs to which [^{18}F]**6** clears liver, kidney, and tumor: (A) organs from mouse that received no tracer (control); (B) organs from mouse injected with **6** at 3.5 Ci/μmol; (C) organs from the mouse injected with **6** at 0.01 Ci/μmol.

dx.doi.org/10.1021/bc5003357 | *Bioconjugate Chem.* 2014, 25, 1951−1962

Table 1. Summary of PET and Fluorescence Data

specific activity (Ci/μmol)	injected dose (μCi)	injected mass (nmol)	initial humoral concentration of tracer in mouse (2 mL blood)	tumor uptake %ID/g (from *in vivo* PET image)	tumor uptake %ID/g (from biodistribution, n = 3)	%ID/g in actual tumor sample	mass in tumor (pmol)	fluorescent detection
3.5	100	0.03	15 nM	5.5	3.8	5.1	0.06	N
0.01	100	10	5 μM	2.5	2.9	3.8	17	Y

detect 60 fmol of tracer within target tissue can be simply explained by the fact that our camera is not sensitive enough to detect fluorescent signal associated with the low mass levels of tracer that is labeled at such high specific activity. Indeed, while others may possess more sensitive cameras, to date, we know of no study where pmol quantities of fluorescent tracer have been injected for fluorescent detection, and furthermore, we know of no study where femtomole quantities of fluorescent probe have been imaged in tumors. Indeed in the vast literature of both fluorescent probes and dual mode tracers, some of which we cite here, it is generally appreciated that 2−10 nmol are typically needed to achieve fluorescence detection, even in best-case scenarios where near-IR fluorophores are used.[55]

What then do these data portend for the use of dual mode tracers in terms of specific activity? If one critically considers injecting 100 μCi of a dual-mode tracer comprising >2 nmol total mass, simple math dictates that the specific activity must fall to <0.05 Ci/μmol, a value that is generally considered to be too low for PET and one that may result in relatively low tumor uptake values, as we have demonstrated herein. Indeed, such a diminution in tumor uptake is the expected consequence of lowering the specific activity, and it is precisely this erosion in image quality that highlights the need for high specific activity. As PET is at least 10-fold more sensitive than fluorescence,[6] the most pregnant implication of these results is that if high specific activity is desired for PET imaging, fluorescence detection limits will need to be significantly improved through advances in camera hardware and/or increases in molar quantum yields (i.e., use of brighter quantum dots or nanoparticles decorated with hundreds of fluorophores).[56] Otherwise, specific activities will need to be kept low, i.e., at <0.05 Ci/μmol in order to provide sufficiently high levels of mass that will ensure fluorescence detection. A trade-off is thus realized: with a much larger mass dose needed for fluorescence, tumor uptake values in the PET image will likely fall. While this trade-off is clearly in evidence herein with a mouse model, we may speculate that for human patients, where 100-fold higher doses (e.g., 10 mCi) are used, it may be possible that tumor uptake may be just at the threshold of fluorescence detection even when tracers are labeled at high specific activity.

The real interest in dual-mode tracers such as **6** may not lie in simultaneous imaging with both modes but for seamless use in two independent aims, whereby one aim requires fluorescence while the other requires very high specific activity. For example, it would be of great utility to use fluorescence to define target status in a biopsy specimen or to screen several tracers on biopsy slides in a multiplexed assay to personalize tracer choice. Fluorescent staining with a dual mode tracer would further confirm that both the radioprosthesis and fluorophore do not interfere with target binding. Following positive histological results, the same dual-mode tracer could be labeled by IEX in a single step to create a PET tracer at very high specific activity for staging disease in the same patient from whom the biopsy sample was removed. Furthermore, once a malignant mass is detected by PET-imaging at high specific activity, the patient could be reinjected with greater quantities of cold tracer to fluorescently label the target in order to guide surgical removal.

Notwithstanding the significant discrepancy between PET and fluorescent detection limits, [^{18}F]**6**, as a PET tracer alone, compares favorably with other RGD tracers. An extensive body of literature reveals that most radiosyntheses achieve lower specific radioactivities (0.5−1 Ci/μmol), while there is a considerable range of uptake values (0.27−12% ID/g) depending on the specific RGD composition.[33,57,58] At both high and low specific activities, [^{18}F]**6** cleared rapidly to the bladder through the kidneys with minimal liver uptake (~4% ID/g) and blockable uptake in bone and other viscera. Interestingly, *in vivo* tumor imaging with uptake values were similar to Al-[^{18}F]-NOTA-bisRGD[48] and 10-fold higher values compared to our previous report on a nonfluorescent dimeric cRGD comprising a different linker along with an anionic [^{18}F]-aryl-BF_3^- prosthesis.[46] While it is likely that the rhodamine retarded clearance, more work will be needed to clarify the respective roles that the rhodamine, the zwitterionic $AMBF_3^-$ prosthesis, and the pentaerythritol scaffold play to increase uptake 10-fold.

CONCLUSION

Here we report a convergent synthetic route to a dual mode fluorescent-PET tracer. At high specific activity, tumor uptake values in the PET image were higher than those at low specific activity. In terms of fluorescence, uptake showed an inverted trend where detection limits prevented fluorescent detection at very high specific activity. Indeed, the specific activity of the PET tracer was so high that the high tumor uptake observed by PET imaging could only be correlated with fluorescent detection by the addition of unlabeled fluorescent tracer in what constituted a partial blocking experiment. In other words, fluorescence imaging is currently incompatible with high specific activity. This work highlights a discrepancy in detection limits between PET and fluorescence that may eventually be resolved through improvements in molar quantum yields, camera hardware, and/or greatly improved tumor uptake (e.g. >50% ID/g). Notwithstanding this discrepancy, applications of dual mode tracers may enable multiple separate applications based on a single mode (*vide supra*). Besides such applications there are several salient attributes of the synthetic method exemplified by **6** that may apply more generally to radiotracer development. These include the following: (1) kit labeling based on ~150 μg of precursor, (2) no azeotropic drying of the [^{18}F]fluoride ion, (3) high yields, (4) high specific activity, and (5) HPLC-free purification within a fully shielded, clinical hot cell, to provide up to 25 human doses within 30 min. Given the broad applicability and bio-orthogonality of click conjugations, synthon **4** should be amenable for grafting many peptides, oligonucleotides (aptamers/siRNAs etc.), as well as a broad range of fluorophores for fine-tuning and/or increasing emission wavelengths while optimizing both target binding and *in vivo* clearance. This scaffold will likely accommodate other prosthetic groups, e.g., [^{18}F]aryltrifluoroborates,[41] [^{18}F]-

dx.doi.org/10.1021/bc5003357 | *Bioconjugate Chem.* 2014, 25, 1951−1962

silyl-fluorides,[59,60] and chelators for chelating aluminum-[^{18}F]fluoride or other radiometals and should find use to generate *in vivo* active "click" reagents containing one more more reactive groups e.g. azides, tetrazines, cyclooctenes, cyclopropenes etc.[61] This synthetic approach should be readily adaptable to creating trimeric peptide tracers without fluorophores along with peptide-linked (radio)toxin theranostics by replacing the fluorophore with a (radio)toxin. Finally, trimodal probes that combine an MRI contrast agent, a fluorophore, and a radioprosthesis are readily envisaged. The present report should empower others to access the combined advantages of peptide dimerization, fluorescence, and one-step aqueous radiofluorination, in a modular and user-friendly manner to expand the palette of fluorescent ^{18}F-labeled radiotracers and related bioconjugates while considering other more baroque constructs.

EXPERIMENTAL PROCEDURES

General Information. Reagents and solvents were purchased from Fischer, Sigma-Aldrich, Combi-Blocks, Novabiochem, or Clicktools. Cell lines were purchased from Stemcell and media from Invitrogen. Deuterated solvents were purchased from Cambridge Isotope Laboratories. [^{18}F]-fluoride Trap & Release Columns were purchased from ORTG Inc. (Oakdale, TN) and C18 Sep-Pak cartridges (1 cm^3, 50 mg) were obtained from Waters. Analytical thin layer chromatography was undertaken on Silica Gel 60 F254 Glass TLC plates from EMD Chemicals and SiliaFlash F60 from Silicycle was used for flash chromatography. ESI-LRMS was performed on a Waters ZQ with a single quadrupole detector, attached to a Waters 2695 HPLC. ESI-HRMS was obtained on a Waters-Micromass LCT with a time-of-flight (TOF) detector. All NMR spectra were recorded at room temperature on a Bruker Avance 300 or 400 MHz spectrometer. Chemical shifts are reported using the δ scale in ppm and all coupling constants (J) are reported in hertz (Hz). Unless specified, ^{1}H NMR spectra are referenced to the tetramethylsilane peak (δ = 0.00 ppm), ^{13}C NMR spectra are referenced to the chloroform peak (δ = 77.23 ppm), and ^{19}F NMR spectra are referenced to neat trifluoroacetic acid (δ = 0.00 ppm, −78.3 ppm relative to $CFCl_3$). HPLC analysis was performed on the Agilent 1100 HPLC system equipped with an autoinjector, a fraction collector, and a diode array detector (nonradiolabeling) or on an Agilent 1200 series with a variable wavelength detector and Bioscan radioactivity NaI detector (radiolabeling). Phenomenex Jupiter 10 μ C18 300 Å 4.6 mm × 250 mm column (Column I) was used for analysis or separation of the radiolabeling reaction and Agilent Eclipse XDB-C18 5 μ 9.4 mm × 250 mm column (Column II) was used for semipreparative HPLC.

HPLC Methods. *Gradient A.* Agilent Eclipse XDB-C18 5 μm 9.2 × 250 mm semiprep column. Solvent A: 0.1% TFA water; solvent B: MeCN; 0 to 2 min: 5% to 5% B, 2 to 7 min, 5% to 35% B, 7 to 15 min, 35% to 65%, 15 to 20 min, 65% to 100% B. Flow rate: 3 mL/min, column temperature: 19 to 21 °C.

Gradient B. Agilent Eclipse XDB-C18 5 μm 9.2 × 250 mm semiprep column. Solvent A: 0.1% TFA water; solvent B: MeCN; 0 to 2 min: 5% to 20% B, 2 to 5 min, 20% to 30% B, 5 to 20 min, 30% to 100%, 20 to 22 min, 100% to 5% B. Flow rate: 3 mL/min, column temperature: 19 to 21 °C.

Gradient C. Phenomenex Jupiter 10 μ C18 300 Å 4.6 × 250 mm analytical column. Solvent A: 0.1% TFA water; solvent B: MeCN; 0 to 2 min: 5% to 5% B, 2 to 7 min, 5% to 20% B, 7 to 15 min, 20% to 100%, 15 to 20 min, 100% to 5% B. Flow rate: 2 mL/min, column temperature: 19 to 21 °C.

Synthesis of 3-(Prop-2-yn-1-yloxy)-2,2-bis((prop-2-yn-1-yloxy)methyl)propan-1-ol (1). 2.00 g (14.7 mmol) of pentaerythritol was suspended in DMSO (15 mL). A solution of 40% NaOH (10 mL) was added dropwise over approximately 30 min. A solution of 80% propargyl bromide in toluene (5 mL, 47.0 mmol) was added dropwise via syringe. The mixture is then stirred overnight for approximately 20 h. Diethyl ether (100 mL) was added and the ether layer was washed with water (25 mL) four successive times. The ether and toluene were then removed via rotary evaporation and the product purified by flash column chromatography (1:1 diethyl ether:petroleum ether). 30% yield (1.12 g, 4.47 mmol). ^{1}H NMR (300 MHz, $CDCl_3$) δ 4.14 (d, J = 2.4 Hz, 6H), 3.70 (d, J = 6.5 Hz, 2H), 3.57 (s, 6H), 2.42 (t, J = 2.4 Hz, 3H); ESI: calculated: 250.3; found: 250.4.

Synthesis of *N,N*-Dimethyl-2-(3-(prop-2-yn-1-yloxy)-2,2-bis((prop-2-yn-1-yloxy) methyl)propoxy)ethan-1-amine (2). Compound **1** (626 mg, 2.50 mmol) was dissolved in DMSO (3 mL), to which 40% NaOH (2 mL) was added. The solution became quite yellow. The hydrochloride salt of *N,N*-dimethylaminoethyl chloride (720 mg, 5.00 mmol) was added. The pH was verified by spotting a small amount of the crude reaction on pH paper; we found that the addition of small amounts of excess NaOH was required to ensure alkaline pH (pH > 12). The mixture was stirred for 3 days. A volume of water (25 mL) was added and the product extracted into diethyl ether 3 × 5 mL each. The product was then extracted into the aqueous phase from the combined ether extracts (3 × 5 mL of 1 M HCl). The combined aqueous extracts were then basified to pH 13 by the addition of concentrated NaOH and the product was extracted into diethyl ether (3 × 5 mL). The ethereal extract was concentrated by rotary evaporation to give the product as yellow oil in 38% yield (308 mg, 0.96 mmol). ^{1}H NMR (300 MHz, $CDCl_3$) δ 4.11 (d, J = 2.4 Hz, 6H), 3.52 (m, 8H), 3.42 (s, 2H), 2.49 (t, J = 5.9 Hz, 2H), 2.39 (t, J = 2.4 Hz, 3H), 2.26 (s, 6H). ^{13}C NMR (300 MHz, CD_3CN) δ 81.0, 75.6, 70.9, 70.4, 69.9, 59.4, 59.3, 46.2, 45.6; ESI: calculated: 321.2; found; 321.4.

Synthesis of *N,N*-Dimethyl-2-(3-(prop-2-yn-1-yloxy)-2,2-bis((prop-2-yn-1-yloxy) methyl)propoxy)-*N*-((4,4,5,5-tetramethyl-1,3,2-dioxaborolan-2-yl) methyl)-ethan-1-ammonium iodide (3). Iodomethylpinacolboronate (165 μL, 0.9 mmol)[62] was dissolved in 3 mL of anhydrous diethyl ether in a flame-dried round-bottom flask under argon atmosphere. Compound **2** (300 mg, 0.93 mmol), isolated as an oil, was dissolved in a minimum amount of anhydrous diethyl ether and added via syringe to the solution of iodomethylpinacolboronate. On stirring, the solution became turbid followed by the formation of an anomalous emulsion. Following stirring overnight, the mixture appeared to form two layers: an oil on the bottom and a clear ethereal layer on top. The diethyl ether was carefully decanted from the viscous oil on the bottom, and fresh diethyl ether (1 mL) was added and the oil triturated. This trituration procedure, for which a sonicator proved useful, was repeated twice for a total of three times. Following trituration, a much more viscous oil was obtained. The residue was then dried under high vacuum to give a yellow product of a thick gel/glass-like consistency in 91% yield (530 mg, 0.82 mmol). ^{1}H NMR (300 MHz, CD_3CN) δ 4.11 (d, J = 2.4 Hz, 6H, 3.79 (br, 2H), 3.56 (t, J = 4.6 Hz, 2H), 3.45 (m, 8H), 3.21 (s, 2H), 3.16 (s, 6H), 2.72 (t, J = 2.4 Hz, 3H), 1.31 (s, 12H).

^{13}C NMR (300 MHz, CD_3CN) δ 86.4, 80.8, 75.8, 71.2, 69.8, 66.6, 66.0, 59.2, 55.3, 45.2, 24.9; ESI: calculated: 462.2; found: 462.4. HRMS $[M]^+$ calculated: 461.3063, found: 461.3058.

Synthesis of *N*-((trifluoroborato)methyl)-*N*,*N*-dimethyl-2-(3-(prop-2-yn-1-yloxy)-2,2-bis((prop-2-yn-1-yloxy)-methyl)propoxy)ethan-1-ammonium (4). A 1.5 mL Eppendorf tube was charged with DMF (80 μL) into which was dissolved compound **3** (5.0 mg, 8.48 μmol). To this were added in the following order: 3 M KHF_2 (40 μL), 4 M HCl (20 μL), and H_2O (20 μL). The solution was then mixed by vigorous vortexing and left to stand for 20 h. The reaction was then concentrated to apparent dryness in vacuo via speed-vac at 65 °C. The residue was then resuspended in 10% MeOH in CH_2Cl_2 (100 μL) and purified flash silica chromatography (0.3 cm × 5 cm in a Pasteur pipet), using 10% MeOH/CH_2Cl_2. R_f = 0.57 (10% MeOH/CH_2Cl_2) to afford the product in 94% yield (3.2 mg, 7.94 μmol). ^{1}H NMR (300 MHz, $CDCl_3$) δ 4.11 (d, J = 2.4 Hz, 6H), 3.84 (t, J = 4.4 Hz, 2H), 3.51 (t, J = 4.4 Hz, 2H), 3.47 (m, 8H), 3.16 (s, 6H), 2.56 (br, 2H), 2.43 (t, J = 2.4 Hz, 3H). ^{13}C NMR (300 MHz, CD_3CN) δ 80.9, 75.7, 70.9, 69.8, 66.6, 66.3, 59.3, 55.0, 45.4. ^{19}F NMR (300 MHz, $CDCl_3$) δ −139.7; ESI: calculated 403.2; found: 403.3. HRMS $[M]^+$ calculated: 425.2076, found: 425.2073.

Synthesis of Rhodamine-Bisalkyne-^{19}F-AMBF$_3$ (5). This reaction was run several times at the scale reported here. A 1.5 mL Eppendorf tube was charged with compound **4** (10 mg, 24.5 μmol), Rhodamine-triethylene glycol-bis-sulfonate-568-azide, obtained from Click tools: λ_{max} 568 nm, ε_M 100 000 M^{-1} cm^{-1})[27,28] (5 mg, 6.6 μmol), aqueous $CuSO_4$ (1.0 M, 5 μL), and sodium ascorbate (1.0 M, 12.5 μL) and (5% NH_4OH in MeCN:H_2O − 1:1, 50 μL). This mixture was reacted at 45 °C for 2 h and then directly loaded onto a semipreparative HPLC column and purified (Gradient A, T_R = 12.1 min) to yield chemically pure rhodamine-bisalkynyl-^{19}FAMBF$_3^{-2}$ in 60% yield (4.5 mg, 3.9 μmol). The fractions containing **5** were pooled and the concentration is determined by first measuring the absorbance at 568 nm and dividing by the molar extinction coefficient. Portions corresponding to 1 μmol were lyophilized *in vacuo* and stored as aliquots at −20 °C for further conjugation. ESI: Calculated: 1161.49; Obtained: 1161.5.

Synthesis of Rhodamine-bisRGD-^{19}F-AMBF$_3$ (6). Several reactions were carried out under identical conditions below to provide 1 mg of **6** as needed. For a typical reaction, in a 1.5 mL Eppendorf tube, compound **5** (1.2 mg, 1.0 μmol) is dissolved in 30 μL of 5% NH_4OH in MeCN/H_2O = 1:1. To this is added RGD-azide (3 mg, 4.8 μmol in water), $CuSO_4$ (1.0 M in water, 3 μL), and sodium ascorbate (1.0 M in water, 7.5 μL). This mixture is allowed to react at 45 °C for 2 h, and then directly loaded onto a semipreparative HPLC column and purified by HPLC (Gradient B, T_R = 11.2 min), to yield chemically pure rhodamine-bisRGD-^{19}F-AMBF$_3^-$ in 41% yield (1 mg, 0.41 μmol). The identity and purity was confirmed with MALDI-TOF spectrometry: Calculated: 2421.1; Found: 2421.3. Following lyophilization the solution was resuspended in ∼200 μL ethanol to give a solution of 2.1 μM. Following serial dilutions, the concentration was confirmed by UV−vis spectroscopy using the extinction coefficient of at 568 nm. Aliquots of 50 nmol (121 μg) or 75 nmol (181 μg) were prepared, lyophilized, and stored at −20 °C for further use.

Cell Based Assays. HT29 cells are grown in McCoy 5A media with 10% FBS, and 2 mM L-glutamine. U87 M cells were grown in DMEM supplemented with 10% FBS and 2 mM L-glutamine. For visualization by fluorescent microscopy, cells in 100 μL 10% fetal calf serum were incubated in the presence of **6** (480 nM for U87 M cells, positive control, or 960 nM − for HT29 cells, negative control). Following 1 h, the cells were briefly washed twice with PBS to which was applied 1 drop Dako fluorescent mounting medium, and a coverslip. Cells were visualized at 20× using a Lecia 6000B microscope. Image is inverted for clarity.

Radiolabeling. Radiolabeling generally followed previous reports on this method.[28,29] Briefly, [^{18}F]fluoride ion was obtained from the bombardment of ^{18}O−H_2O with 18 MeV protons in a niobium target and transferred to the hot cell through a preactivated QMA anion trap (9 mg of matrix, chloride form) that was pretreated with 6 mL deionized water, 6 mL saturated brine (NaCl), followed by 6 mL deionized water to convert it to the chloride form of the resin. Approximately 1.5 mL of target water containing 800−1200 mCi was transferred within a shielded hot cell to the anion exchange resin. Then >90% radioactivity was eluted with 70−100 μL 0.9% isotonic saline into a polypropylene Falcon tube that had been fitted with a septum and which contained an aliquot of **6** (50 or 75 nmol) that had been resuspended in 30 μL of DMF and 30 μL aqueous buffer pH 2 as previously detailed just prior to bombardment.[28,29] The tube containing the labeling reaction was then placed in a heated sand bath (85 °C) for 20 min whereupon 2 mL of quench solution (5% NH_4OH in pure water) was added to the reaction by syringe. The entire reaction contents were then withdrawn into a 3 mL syringe and passed over a reverse phase C18-Sep-Pak which was then washed with 2 mL saline. The tracer was then eluted into a sterile capped vial by passage of 2 mL of 1:1 ethanol−PBS. Radiochemical yields of 11−33% were achieved (n = 3).

Serum Stability Assay. This protocol follows our previous reports that were developed for labeled bombesin.[63] Here, [^{18}F]**6**, (∼2 mCi) in 50% PBS-EtOH was further diluted in saline buffer (0.5 mL). For each assay, the saline solution (100 μL) was mixed with plasma (100 μL), incubated at 37 °C for 0, 60, and 120 min, and quenched by the addition of 75% aqueous CH_3CN (400 μL). The resulting mixture was vortexed and then centrifuged at 13 krpm for 20 min to precipitate insoluble components. The supernatant was then decanted, filtered (0.22 μm), and analyzed by HPLC (Gradient C) which indicates that there is no detectable defluorination (T_R ∼ 2.5 min) or other degradation products (see Supporting Information).

Specific Activity Measurement. To assess the specific activity, a standard curve (see Supporting Information) was achieved by chromatographing a series of known quantities unlabeled **6** by HPLC (Gradient 3). The exact quantity of each injection was previously determined by absorbance at 568 nm of the stock solution. For the radiosynthesis (Figure 3B), integration of the visible peak (568 nm) that eluted at 12.5 min provided a quantitative mass value of 0.46 nmol based on the fitted linear standard curve. For the reinjection (Figure 3B) 2 mCi [^{18}F]**6** was loaded on HPLC and 1.8 mCi of the radioactivity was collected at 12.5 min. Hence, the specific activity was measured to be 3.95 Ci/μmol at the time of collection. The same experiments were repeated three times (see Supporting Information for results).

Animal Care and in Vivo Image Acquisition. The methods detailed in relation to animals are similar to those we previously reported for imaging RGD in U87 M xenograft tumors.[46] Briefly, all animal studies were performed in accordance with the Canadian Council on Animal Care Guidelines and were reviewed and approved by the University

of British Columbia Animal Care Committee. Rag2M mice (8–11 weeks old, bred in-house at the BC Cancer Research Agency) were subcutaneously inoculated with U87 M (human glioblastoma) cells into the lower back (5×10^6 cells). The tumors were grown to a suitable size (~100 mm^3) within approximately 2 weeks and were measured by calipers. Mice were anesthetized by 2% isofluorane inhalation. For biodistribution studies in mice with tumors, the tracer was injected via the lateral tail vein with a catheter while mice were under anesthesia. Eight mice were used, four of which received 100 μCi [^{18}F]**6** at 3.5 Ci/μmol, while four were set aside for a partial blocking experiment where they received 100 μCi of [^{18}F]**6** at 0.01 Ci/μmol. Prior to *ex vivo* biodistribution, one set of paired, tumor-bearing mice (unblocked and partially blocked) were imaged using the Siemens Inveon multimodality small animal PET/CT scanner to evaluate the tumor-to nontarget-tissue contrast for the tracer. A 10 min CT attenuation scan followed by a 120 min Dynamic PET scan was carried out. The list-mode data were histogrammed, and reconstructed by an iterative reconstruction algorithm (3D OSEM/MAP) using the Inveon Acquisition Workplace Software (Siemens), applying normalization, dead time, random, and attenuation correction. The attenuation correction map was obtained from the CT scan data. Images representing pure-PET are shown in the Supporting Information demonstrate the lack of bone uptake. Time activity curves were also generated using the images with ROIs placed in the tissue of interest. For bone analysis, the ROI was placed in the femur and for muscle analysis, the ROI was placed in the fleshy part of the hind leg.

Biodistribution Analysis. These methods largely follow our previous reports on RGD and dimeric versions thereof.[29,46] Briefly, following scanning, all mice were humanely euthanized by isofluorane overdose followed by CO_2 inhalation and tissues/organs of interest were collected, rinsed in PBS, patted dry, and counted in a gamma counter (Cobra-II Auto Gamma, Canberra Packard Canada). The tissue weight and associated cpm (counts per min) were used to calculate the percentage of injected dose per gram of tissue (%ID/g) with decay correction. The biodistribution data are shown in the Supporting Information.[46−48] Hence errors on tumor uptake are not expected to be statistically significant.

Ex Vivo Fluorescence Analysis. Since the PET imaging data had indicated that [^{18}F]**6** was taken up in the tumor and otherwise cleared predominantly to the liver or the bladder via the kidneys, portions of liver, kidney, and tumor were further analyzed for fluorescence using a Maestro-2 imaging station. Tissues were excited at 568−570 nm and fluorescent images were acquired at an exposure time of 1 s. Organs from the control animal, which did not receive the fluorescent tracer, were used to determine background levels of autofluorescence at the wavelengths used. Images for the various organs were obtained under the same exposure conditions.

■ ASSOCIATED CONTENT

Supporting Information

Serum stability data, Maldi-TOF trace, and standard curve analysis. This material is available free of charge via the Internet at http://pubs.acs.org.

■ AUTHOR INFORMATION

Corresponding Author

*E-mail: dperrin@chem.ubc.ca.

Notes

The authors declare the following competing financial interest(s): UBC has filed a patent application on the radioprosthesis used in this work.

■ ACKNOWLEDGMENTS

This work was supported by NSERC and by funds from the CCSRI #27001 and by SOF funds from Genome B.C.

■ REFERENCES

(1) Culver, J., Akers, W., and Achilefu, S. (2008) Multimodality molecular imaging with combined optical and SPECT/PET modalities. *J. Nucl. Med. 49*, 169−172.

(2) Kuil, J., Velders, A. H., and van Leeuwen, F. W. B. (2010) Multimodal tumor-targeting peptides functionalized with both a radio- and a fluorescent label. *BioconjugateChem. 21*, 1709−1719.

(3) van der Poel, H. G., Buckle, T., Brouwer, O. R., Olmos, R. A. V., and van Leeuwen, F. W. B. (2011) Intraoperative laparoscopic fluorescence guidance to the sentinel lymph node in prostate cancer patients: clinical proof of concept of an integrated functional imaging approach using a multimodal tracer. *Eur. Urol. 60*, 826−833.

(4) Banerjee, S. R., Pullambhatla, M., Byun, Y., Nimmagadda, S., Foss, C. A., Green, G., Fox, J. J., Lupold, S. E., Mease, R. C., and Pomper, M. G. (2011) Sequential SPECT and optical imaging of experimental models of prostate cancer with a dual modality inhibitor of the prostate-specific membrane antigen. *Angew. Chem., Int. Ed. 50*, 9167−9170.

(5) Lee, H., Akers, W. J., Cheney, P. P., Edwards, W. B., Liang, K., Culver, J. P., and Achilefu, S. (2009) Complementary optical and nuclear imaging of caspase-3 activity using combined activatable and radio-labeled multimodality molecular probe. *J. Biomed. Opt. 14*, 0405071−3.

(6) Nahrendorf, M., Keliher, E., Marinelli, B., Waterman, P., Feruglio, P. F., Fexon, L., Pivovarov, M., Swirski, F. K., Pittet, M. J., Vinegoni, C., and Weissleder, R. (2010) Hybrid PET-optical imaging using targeted probes. *Proc. Natl. Acad. Sci. U.S.A. 107*, 7910−7915.

(7) te Velde, E. A., Veerman, T., Subramaniam, V., and Ruers, T. (2010) The use of fluorescent dyes and probes in surgical oncology. *Ejso 36*, 6−15.

(8) Sevick-Muraca, E. M. (2012) Translation of near-infrared fluorescence imaging technologies: emerging clinical applications, in *Annual Review of Medicine* (Caskey, C. T., Austin, C. P., and Hoxie, J. A., Eds.) pp 217−231, Vol *63*, Annual Reviews, Palo Alto.

(9) Houston, J. P., Ke, S., Wang, W., Li, C., and Sevick-Muraca, E. M. (2005) Quality analysis of in vivo near-infrared fluorescence and conventional gamma images acquired using a dual-labeled tumor-targeting probe. *J. Biomed. Opt. 10*, 0540101−3.

(10) Kimura, R. H., Miao, Z., Cheng, Z., Gambhir, S. S., and Cochran, J. R. (2010) A dual-labeled knottin peptide for PET and near-infrared fluorescence imaging of integrin expression in living subjects. *BioconjugateChem. 21*, 436−444.

(11) Azhdarinia, A., Ghosh, P., Ghosh, S., Wilganowski, N., and Sevick-Muraca, E. M. (2012) Dual-labeling strategies for nuclear and fluorescence molecular imaging: a review and analysis. *Mol. Imag. Biol. 14*, 261−276.

(12) Cai, L. S., Lu, S. Y., and Pike, V. W. (2008) Chemistry with F-18 fluoride ion. *Eur. J. Org. Chem.*, 2853−2873.

(13) Smith, G. E., Sladen, H. L., Biagini, S. C. G., and Blower, P. J. (2011) Inorganic approaches for radiolabelling biomolecules with fluorine-18 for imaging with positron emission tomography. *Dalton Trans. 40*, 6196−6205.

(14) Smith, G., Carroll, L., and Aboagye, E. O. (2012) New frontiers in the design and synthesis of imaging probes for PET oncology: current challenges and future directions. *Mol. Imag. Biol. 14*, 653−666.

(15) Hudnall, T. W., Lin, T. P., and Gabbai, F. P. (2010) Substitution of hydroxide by fluoride at the boron center of a BODIPY dye. *J. Fluor. Chem. 131*, 1182−1186.

(16) Hendricks, J. A., Keliher, E. J., Wan, D. P., Hilderbrand, S. A., Weissleder, R., and Mazitschek, R. (2012) Synthesis of F-18 BODIPY: bifunctional reporter for hybrid optical/positron emission tomography imaging. *Angew. Chem., Int. Ed. 51*, 4603−4606.
(17) Li, Z. B., Lin, T. P., Liu, S. L., Huang, C. W., Hudnall, T. W., Gabbai, F. P., and Conti, P. S. (2011) Rapid aqueous F-18 -labeling of a bodipy dye for positron emission tomography/fluorescence dual modality imaging. *Chem. Commun. 47*, 9324−9326.
(18) Liu, S. L., Lin, T. P., Li, D., Leamer, L., Shan, H., Li, Z. B., Gabbai, F. P., and Conti, P. S. (2013) Lewis acid-assisted isotopic F-18-F-19 exchange in BODIPY dyes: facile generation of positron emission tomography/fluorescence dual modality agents for tumor imaging. *Theranostics 3*, 181−189.
(19) Ting, R., Aguilera, T. A., Crisp, J. L., Hall, D. J., Eckelman, W. C., Vera, D. R., and Tsien, R. Y. (2010) Fast F-18 labeling of a near-infrared fluorophore enables positron emission tomography and optical imaging of sentinel lymph nodes. *Bioconjugate Chem. 21*, 1811−1819.
(20) Pauwels, E. K. J., Bergstrom, K., Mariani, G., and Kairemo, K. (2009) Microdosing, imaging biomarkers and SPECT: a multi-sided tripod to accelerate drug development. *Curr. Pharm. Des. 15*, 928−934.
(21) Gomes, C. M. F., Abrunhosa, A. J., and Pauwels, E. K. J. (2011) Molecular imaging with SPECT and PET in exploratory investigational new drug studies. *Drugs of the Future 36*, 69−77.
(22) Lapi, S. E., and Welch, M. J. (2012) A historical perspective on the specific activity of radiopharmaceuticals: what have we learned in the 35 years of the ISRC? *Nucl. Med. Biol. 39*, 601−608.
(23) Chopra, A., Shan, L., Eckelman, W. C., Leung, K., and Menkens, A. E. (2011) Important parameters to consider for the characterization of PET and SPECT imaging probes. *Nucl. Med. Biol. 38*, 1079−1084.
(24) Eckelman, W. C., Bonardi, M., and Volkert, W. A. (2008) True radiotracers: are we approaching theoretical specific activity with Tc-99m and I-123? *Nucl. Med. Biol. 35*, 523−527.
(25) Carlucci, G., Ananias, H. J. K., Yu, Z. L., Van de Wiele, C., Dierckx, R. A., de Jong, I. J., and Elsinga, P. H. (2012) Multimerization improves targeting of peptide radio-pharmaceuticals. *Curr. Pharm. Des. 18*, 2501−2516.
(26) Yim, C. B., van der Wildt, B., Dijkgraaf, I., Joosten, L., Eek, A., Versluis, C., Rijkers, D. T. S., Boerman, O. C., and Liskamp, R. M. J. (2011) Spacer effects on in vivo properties of DOTA-conjugated dimeric Tyr3 octreotate peptides synthesized by a ″Cu-I-Click″ and ″Sulfo-Click″ ligation method. *ChemBioChem 12*, 750−760.
(27) Liu, Z. B., Li, Y., Lozada, J., Schaffer, P., Adam, M. J., Ruth, T. J., and Perrin, D. M. (2013) Stoichiometric leverage: rapid ^{18}F-aryltrifluoroborate radiosynthesis at high specific activity for click conjugation. *Angew. Chem., Int. Ed. 52*, 2303−2307.
(28) Liu, Z., Li, Y., Lozada, J., Lin, K.-S., Schaffer, P., and Perrin, D. M. (2012) Rapid, one-step, high yielding ^{18}F-labeling of an aryltrifluoroborate bioconjugate by isotope exchange at very high specific activity. *J. Labelled Compd. Radiopharm. 14*, 491−97.
(29) Liu, Z., Li, Y., Lozada, J., Wong, M. Q., Greene, J., Lin, K.-S., Yapp, D., and Perrin, D. M. (2013) Kit-like ^{18}F-labeling of RGD-19F-Arytrifluroborate in high yield and at extraordinarily high specific activity with preliminary in vivo tumor imaging. *Nucl. Med. Biol. 40*, 841−849.
(30) Li, Z. B., Chansaenpak, K., Liu, S. L., Wade, C. R., Conti, P. S., and Gabbai, F. P. (2012) Harvesting F-18-fluoride ions in water via direct F-18-F-19 isotopic exchange: radiofluorination of zwitterionic aryltrifluoroborates and in vivo stability studies. *MedChemComm 3*, 1305−1308.
(31) Chin, F. T., Shen, B., Liu, S. L., Berganos, R. A., Chang, E., Mittra, E., Chen, X. Y., and Gambhir, S. S. (2012) First experience with clinical-grade F-18 FPP(RGD)(2): an automated multi-step radiosynthesis for clinical PET studies. *Mol. Imaging Biol. 14*, 88−95.
(32) Wan, W., Guo, N., Pan, D., Yu, C., Weng, Y., Luo, S., Ding, H., Xu, Y., Wang, L., Lang, L., Xie, Q., Yang, M., and Chen, X. (2013) First experience of F-18-alfatide in lung cancer patients using a new lyophilized kit for rapid radiofluorination. *J. Nucl. Med. 54*, 691−698.
(33) Liu, S. (2009) Radiolabeled cyclic RGD peptides as integrin alpha(v)beta(3)-targeted radiotracers: maximizing binding affinity via bivalency. *Bioconjugate Chem. 20*, 2199−2213.
(34) Zhang, X. F., Zhang, Y. K., and Liu, L. M. (2014) Fluorescence lifetimes and quantum yields of ten rhodamine derivatives: Structural effect on emission mechanism in different solvents. *J. Lumin. 145*, 448−453.
(35) Peng, X. X., Chen, H. X., Draney, D. R., Volcheck, W., Schutz-Geschwender, A., and Olive, D. M. (2009) A nonfluorescent, broad-range quencher dye for Forster resonance energy transfer assays. *Anal. Biochem. 388*, 220−228.
(36) Rostovtsev, V. V., Green, L. G., Fokin, V. V., and Sharpless, K. B. (2002) A stepwise Huisgen cycloaddition process: Copper(I)-catalyzed regioselective ″ligation″ of azides and terminal alkynes. *Angew. Chem., Int. Ed. 41*, 2596−+.
(37) Wu, P., Malkoch, M., Hunt, J. N., Vestberg, R., Kaltgrad, E., Finn, M. G., Fokin, V. V., Sharpless, K. B., and Hawker, C. J. (2005) Multivalent, bifunctional dendrimers prepared by click chemistry. *Chem. Commun.*, 5775−5777.
(38) Wang, Q., Chan, T. R., Hilgraf, R., Fokin, V. V., Sharpless, K. B., and Finn, M. G. (2003) Bioconjugation by copper(I)-catalyzed azide-alkyne 3 + 2 cycloaddition. *J. Am. Chem. Soc. 125*, 3192−3193.
(39) Marik, J., and Sutcliffe, J. L. (2006) Click for PET: rapid preparation of F-18 fluoropeptides using Cu-I catalyzed 1,3-dipolar cycloaddition. *Tetrahedron Lett. 47*, 6681−6684.
(40) Moses, J. E., and Moorhouse, A. D. (2007) The growing applications of click chemistry. *Chem. Soc. Rev. 36*, 1249−1262.
(41) Li, Y., Guo, J., Tang, S., Lang, L., Chen, X., and Perrin, D. M. (2013) One-step and one-pot-two-step radiosynthesis of cyclo-RGD-18F-aryltrifluoroborate conjugates for functional imaging. *Am. J. Nucl. Med. Mol. Imag. 3*, 44−56.
(42) Cai, W. B., Chen, K., Li, Z. B., Gambhir, S. S., and Chen, X. Y. (2007) Dual-function probe for PET and near-infrared fluorescence imaging of tumor vasculature. *J. Nucl. Med. 48*, 1862−1870.
(43) Wang, W., Ke, S., Kwon, S., Yallampalli, S., Cameron, A. G., Adams, K. E., Mawad, M. E., and Sevick-Muraca, E. M. (2007) A new optical and nuclear dual-labeled imaging agent targeting interleukin 11 receptor alpha-chain. *Bioconjugate Chem. 18*, 397−402.
(44) Hughes, D. E., Salter, D. M., Dedhar, S., and Simpson, R. (1993) Integrin expression in human bone. *J. Bone Miner. Res. 8*, 527−533.
(45) Schaffner, P., and Dard, M. M. (2003) Structure and function of RGD peptides involved in bone biology. *Cell. Mol. Life Sci. 60*, 119−132.
(46) Li, Y., Liu, Z. B., Lozada, J., Wong, M. Q., Lin, K. S., Yapp, D., and Perrin, D. M. (2013) Single step F-18-labeling of dimeric cycloRGD for functional PET imaging of tumors in mice. *Nucl. Med. Biol. 40*, 959−966.
(47) Li, W. H., Lang, L. X., Niu, G., Guo, N., Ma, Y., Kiesewetter, D. O., Shen, B. Z., and Chen, X. Y. (2012) N-Succinimidyl 4- F-18 -fluoromethylbenzoate-labeled dimeric RGD peptide for imaging tumor integrin expression. *Amino Acids 43*, 1349−1357.
(48) Guo, N., Lang, L. X., Li, W. H., Kiesewetter, D. O., Gao, H. K., Niu, G., Xie, Q. G., Chen, X. Y. (2012) Quantitative analysis and comparison study of F-18 AlF-NOTA-PRGD2, 18F FPPRGD2 and Ga-68 Ga-NOTA-PRGD2 using a reference tissue model. *PLoS One 7*.
(49) Cheng, Z., Wu, Y., Xiong, Z. M., Gambhir, S. S., and Chen, X. Y. (2005) Near-infrared fluorescent RGD peptides for optical imaging of integrin alpha(v)beta 3 expression in living mice. *BioconjugateChem. 16*, 1433−1441.
(50) Wu, Y., Cai, W. B., and Chen, X. Y. (2006) Near-infrared fluorescence imaging of tumor integrin alpha(v)beta(3) expression with Cy7-labeled RGD multimers. *Mol. Imag. Biol. 8*, 226−236.
(51) Adams, K. E., Ke, S., Kwon, S., Liang, F., Fan, Z., Lu, Y., Hirschi, K., Mawad, M. E., Barry, M. A., and Sevick-Muraca, E. M. (2007) Comparison of visible and near-infrared wavelength-excitable fluorescent dyes for molecular imaging of cancer. *J. Biomed. Opt. 12*, 024017.
(52) Huang, R. M., Vider, J., Kovar, J. L., Olive, D. M., Mellinghoff, I. K., Mayer-Kuckuk, P., Kircher, M. F., and Blasberg, R. G. (2012)

Integrin alpha(v)beta(3)- Targeted IRDye 800CW Near-Infrared Imaging of Glioblastoma. *Clin. Canc. Res. 18*, 5731−5740.
(53) Choi, H. S., Gibbs, S. L., Lee, J. H., Kim, S. H., Ashitate, Y., Liu, F. B., Hyun, H., Park, G., Xie, Y., Bae, S., Henary, M., and Frangioni, J. V. (2013) Targeted zwitterionic near-infrared fluorophores for improved optical imaging. *Nat. Biotechnol. 31*, 148−153.
(54) Cao, J., Wan, S. N., Tian, J. M., Li, S. W., Deng, D. W., Qian, Z. Y., and Gu, Y. Q. (2012) Fast clearing RGD-based near-infrared fluorescent probes for in vivo tumor diagnosis. *Contr. Med. Mol. Imag. 7*, 390−402.
(55) Darne, C., Lu, Y. J., and Sevick-Muraca, E. M. (2014) Small animal fluorescence and bioluminescence tomography: a review of approaches, algorithms and technology update. *Phys. Med. Biol. 59*, R1−60.
(56) Qin, Z. T., Hall, D. J., Liss, M. A., Hoh, C. K., Kane, C. J., Wallace, A. M., and Vera, D. R. (2013) Optimization via specific fluorescence brightness of a receptor-targeted probe for optical imaging and positron emission tomography of sentinel lymph nodes. *J. Biomed. Opt. 18*, 1013151−2.
(57) Haubner, R., Wester, H. J., Weber, W. A., Mang, C., Ziegler, S. I., Goodman, S. L., Senekowitsch-Schmidtke, R., Kessler, H., and Schwaiger, M. (2001) Noninvasive imaging of alpha(v)beta(3) integrin expression using F-18-labeled RGD-containing glycopeptide and positron emission tomography. *Canc. Res. 61*, 1781−1785.
(58) Namavari, M., Cheng, Z., Zhang, R., De, A., Levi, J., Hoerner, J. K., Yaghoubi, S. S., Syud, F. A., and Gambhir, S. S. (2009) A Novel Method for Direct Site-Specific Radiolabeling of Peptides Using F-18 FDG. *BioconjugateChem. 20*, 432−436.
(59) Schirrmacher, R., Bradtmoller, G., Schirrmacher, E., Thews, O., Tillmanns, J., Siessmeier, T., Buchholz, H. G., Bartenstein, P., Waengler, B., Niemeyer, C. M., and Jurkschat, K. (2006) F-18-labeling of peptides by means of an organosilicon-based fluoride acceptor. *Angew. Chem., Int. Ed. Engl. 45*, 6047−6050.
(60) Wangler, C., Schirrmacher, R., Bartenstein, P., and Wangler, B. (2010) Click-Chemistry Reactions in Radiopharmaceutical Chemistry: Fast & Easy Introduction of Radiolabels into Biomolecules for In Vivo Imaging. *Curr. Med. Chem. 17*, 1092−1116.
(61) Tietze, L. F., and Schmuck, K. (2011) SiFA Azide: A New Building Block for PET Imaging Using Click Chemistry. *Synlett*, 1697−1700.
(62) Matteson, D. S., and Majumdar, D. (1979) IODOMETHANE-BORONIC ESTERS AND AMINOMETHANEBORONIC ESTERS. *J. Organomet. Chem. 170*, 259−264.
(63) Li, Y., Liu, Z., Pourghiasian, M., Lin, K.-S., Schaffer, P., Benard, F., and Perrin, D. M. (2013) Alkyne-18F-ArBF3 for One-Pot Click 18F-Labeling of Bombesin for in vivo PET Imaging of Tumors Expressing the GRP-Receptor. *Am. J. Nucl. Med. Mol. Imag. 3*, 57−70.